Available online at www.sciencedirect.com
SCIENCE DIRECT
Polymer 47 (2006) 569–576
polymer
www.elsevier.com/locate/polymer

Synthesis and interfacial properties of montmorillonite/polypyrrole nanocomposites

Kada Boukerma [a], Jean-Yves Piquemal [a], Mohamed M. Chehimi [a,*], Miroslava Mravčáková [b], Mária Omastová [b], Patricia Beaunier [c]

[a] *Interfaces, Traitements, Organisation et Dynamique des Systèmes (ITODYS), Université Paris 7-Denis Diderot and CNRS (UMR 7086), 1 rue Guy de la Brosse, 75005 Paris, France*

[b] *Polymer Institute, Slovak Academy of Sciences, Dúbravská cesta 9, 842 36 Bratislava, Slovakia*

[c] *Laboratoire de Réactivité de Surface, Université Pierre et Marie Curie, Université Paris 6, 4 place Jussieu, 75252 Paris, Cedex 05, France*

Received 13 May 2005; received in revised form 18 November 2005; accepted 22 November 2005
Available online 9 December 2005

Abstract

Montmorillonite/polypyrrole (MMT/PPy) nanocomposites were prepared by the in situ polymerization of pyrrole in the presence of MMT. The morphology of the MMT/PPy nanocomposites as examined by scanning electron microscopy differs slightly from that of the untreated MMT but markedly from that of polypyrrole. X-ray photoelectron spectroscopy (XPS) showed that the materials have MMT-rich surfaces, an indication that polypyrrole is essentially intercalated in the host clay galleries. The transmission electron microscopy showed, that the interlamellar spacing of the untreated MMT increased from 1.25 to 18.9 nm, when compared to nanocomposite MMT/10.8% PPy. Moreover, XPS highlighted the cation exchange of Na^+ from montmorillonite by K^+ (from the oxidant) and by the positively charged polypyrrole chains. Inverse gas chromatography indicated that the nanocomposites are high surface energy materials with a dispersive contribution to the surface energy (γ_S^d) reaching 200 mJ/m^2 at 150 °C, for a PPy loading of 21.4 wt%. The (γ_S^d) values of the MMT/PPy nanocomposites were correlated to the changes in the specific surface area of the MMT induced by the intercalation of polypyrrole.

Keywords: Polypyrrole; Montmorillonite; Nanocomposites

1. Introduction

Polypyrrole, is the subject of numerous studies due to its good environmental stability and high electrical conductivity. This conductive polymer can be potentially used in batteries, supercapacitors, sensors, anhydrous electrorheological fluids, microwave shielding, and corrosion control [1–3]. The conductivity of PPy, prepared by chemical oxidative polymerization ranges from 10^{-4} to 100 S cm^{-1} depending on the preparation conditions. Pure PPy is brittle, insoluble and infusible, and hence not processable. This led to intensive research on the preparation of a variety of organic–organic and inorganic–organic conducting polymer composites and nanocomposites [4–6].

With the development of nanoscience and nanotechnology during the last decade, considerable attention has been paid to the synthesis and application of clay/polymer nanocomposites. Polyolefins, i.e. polyethylene and polypropylene, are the most frequently used polymer matrices for clay-containing nanocomposites [7–9]. Similarly, conducting polymers were investigated in view of developing novel polymer–clay nanocomposites [10–21]. Particularly, nanocomposites of polypyrrole and montmorillonite are potential fillers for the modification of the mechanical and conducting properties of polypropylene and other insulating polymer matrices [12]. The rationale for using clay–polypyrrole nanocomposites as conductive fillers is that when the nanocomposite is exfoliated, it can create conductive paths within a polymeric matrix at a low conductive polymer loading compared to the use of polypyrrole as a pure conductive phase. Moreover, clay–polypyrrole fillers are mechanically stable and are thus expected to shift the conductivity threshold to lower values, that is down to a polypyrrole mass loading as low as 1% or better, and this is by mechanical mixing with the thermoplastic matrix. If the pure polypyrrole powder is mixed instead with conventional polymer matrices, the conductivity threshold is usually reached for a mass loading of 30–60% [22,23]. Our ongoing research

* Corresponding author. Tel.: +33 1442 768 09; fax: +33 1442 768 14.
E-mail address: chehimi@paris7.jussieu.fr (M.M. Chehimi).

0032-3861/$ - see front matter © 2005 Elsevier Ltd. All rights reserved.
doi:10.1016/j.polymer.2005.11.065

programme aims at optimizing the conditions for the preparation of novel fillers based on polypyrrole in view of obtaining conductive filled conventional polymers for a low mass loading of polypyrrole.

Since polypyrrole nanocomposite materials are potential, novel fillers for thermoplastic matrices [12] and conductive anti-corrosion paints [14], it is, therefore, of fundamental and technological importance to determine their surface chemical composition and surface energy because these physicochemical properties are directly correlated with the strength of the filler–matrix interactions [24,25].

The surface chemical composition can be determined by an appropriate surface analytical technique such as X-ray photoelectron spectroscopy (XPS), whereas the surface energy of powders is best assessed by inverse gas chromatography (IGC). IGC is a unique analytical technique that employs molecular probes to investigate the changes in the surface thermodynamic properties of inorganic (e.g. clays), organic (e.g. polymers) and composite materials [26,27]. Particularly, IGC was employed to determine the surface energy of polypyrrole powders and composites [28]. These studies firmly concluded that polypyrrole is a high-energy material and should thus not be ranked with conventional insulating polymers. However, the surface energy of polypyrrole can be minimized with adsorption of conventional polymers such as poly(methyl methacrylate) and/or poly(vinyl chloride) [29,30]. Conversely, the surface energy of poly(vinyl chloride) powder particles increased if this low energy substrate acts as host for the in situ deposition of polypyrrole [31]. As far as polypyrrole–silica nanocomposites are concerned, it was shown that the surface energy of these materials (at 60–80 °C) is much higher compared to those of the reference polypyrrole bulk powders and the bare silica sols [32]. The increase in the surface energy was attributed to the microporous structure of the nanocomposites.

This paper reports on the interfacial properties of a series of MMT/PPy nanocomposites which were prepared by the in situ polymerization of pyrrole in the presence of MMT substrate. Pure MMT and PPy powders were used as control samples. The surface composition of the nanocomposites was determined by XPS and compared to the bulk composition as assessed by elemental analysis. The well known 'four probe method' was used to estimate the conductivity of PPy and MMT/PPy materials. The surface morphology of the nanocomposites was examined by scanning electron microscopy (SEM). Transmission electron microscopy (TEM) was employed in order to check whether the conducting polymer was intercalated between the clay sheets. The surface energy of the specimens was determined by IGC and the specific surface area with nitrogen physisorption experiments.

2. Experimental

2.1. Materials

Montmorillonite (MMT) was a Wyoming type (American Colloid Company, USA). The chemical composition of MMT in weight percent is: 31.16% Si, 50.17% O, 13.28% Al, 3.25% Mg, 1.20% Na, 0.40% K, and 0.54% Ca. Pyrrole (Merck–Schuchardt, Germany) was purified by distillation under reduced pressure and stored in a refrigerator before use; and the oxidant $K_2S_2O_8$ (Slavus, sro., Slovakia) was used as-received.

2.2. Preparation of MMT/PPy nanocomposites

The suspension of MMT in aqueous solution was treated with ultrasound for 10 min in order to exfoliate MMT. The oxidant, $K_2S_2O_8$, was dissolved in water and added under vigorous stirring. After 15 min pyrrole was inserted dropwise. The oxidant-to-pyrrole molar ratio was 1:2. The oxidative polymerization of pyrrole proceeded for 1 h under stirring which was then stopped and the suspension left to decant for 24 h. The end-products were filtered out, washed with copious amounts of distilled water and dried at 60 °C. The target mass loading of PPy in the MMT/PPy nanocomposites was 5–25 wt%, and the real composition was determined by elemental analysis.

2.3. Nanocomposite characterization

2.3.1. Elemental analysis

The MMT/PPy composition was determined by elemental analysis performed at the Service Central d'Analyse of the CNRS (Vernaison, France). The nitrogen weight percent found for PPy was 15.9%. For the MMT/PPy nanocomposites with 5, 10, 15 and 25% expected PPy loadings, the N% was found to be 0.45, 1.72, 2.12 and 3.4%, respectively.

2.3.2. Conductivity measurements

Dc electrical conductivity of PPy and MMT/PPy powders was measured under pressure 30 MPa by the van der Pauw four contact method in a home-made polyetheretherketone (PEEK) cell. Tesla microvoltmeter–picoammeter BM 545 (Czech Republic) and Metra Blansko multimeter M1T 380 (Czech Republic) were used for the measurements of the electrical current and voltage, respectively.

2.3.3. X-ray photoelectron spectroscopy (XPS)

XPS signals were recorded using a Thermo VG ESCALAB 250 system equipped with a micro-focused, monochromatic Al Kα X-ray source (1486.6 eV) and a magnetic lens which increases the electron acceptance angle and hence the sensitivity. The specimens were pressed against double-sided adhesive tapes mounted on sample holders, and then pumped overnight in the fast-entry lock at 5×10^{-8} mbar before introduction in the analysis chamber. A 650 μm-sized X-ray beam was used at a power of 10 mA × 15 kV. The spectra were acquired in the constant analyzer energy mode, with a pass energy of 150 and 40 eV for the survey and the narrow regions, respectively. Charge compensation was achieved with an electron flood gun combined with an argon ion gun. The argon partial pressure was 2×10^{-8} mbar in the analysis chamber. In the case of the pure PPy and the nanocomposites with

the highest PPy mass loadings, the analyses were carried out without flood gun.

The Avantage software, version 1.85, was used for data digital acquisition and processing. The peak binding energy positions were calibrated by setting the polypyrrole N1s peak at 399.7 eV [33]. In the case of the untreated MMT powder, spectral calibration was achieved by setting the C1s component due to hydrocarbon contamination at 285 eV.

The apparent surface compositions were determined by considering the integrated areas of the core-level peaks and their respective sensitivity factors.

2.3.4. Inverse gas chromatography (IGC)

Teflon columns (1/8 in. outer diameter, 15–30 cm long) were packed with MMT/PPy, MMT and PPy powder particles (210–844 mg depending on the material) by the tap-and-fill method. The columns were plugged with glass wool at both ends.

A Hewlett Packard HP6890 fitted with a flame ionization detector (FID) was used for GC measurements. The nitrogen (Air Liquide) carrier gas flow rate was set at 25 cm^3/min. The injector and detector temperatures were 120 and 200 °C, respectively.

Methane (Fluka) was the non-interacting marker used to determine the dead retention time of the columns. Heptane (C7, Acros), octane (C8, Aldrich), nonane (C9, Acros), and decane (C10, Fluka) were used as-received.

The columns were activated at the oven temperature (150 and 180 °C) overnight prior to IGC characterization. Air-probe vapour mixtures (1–5 μl) were injected manually, at infinite dilution, by an SGE gas-tight syringe. The retention times were determined at the peak maxima.

2.3.5. Scanning electron microscopy (SEM)

SEM micrographs were obtained with a Cambridge 120 that is completely controlled from a computer workstation. The filament is a zirconated tungsten and the accelerating voltage was set at 20 kV. All specimens were coated with gold prior to analysis in order to avoid or limit static charging effects.

2.3.6. Transmission electron microscopy (TEM)

Transmission electron microscopy (TEM) micrographs were obtained using a JEOL JEM 100CXII UHR operating at 100 kV. The MMT/PPy samples were embedded in an epoxy resin, cured for 48 h at 60 °C. The TEM samples were prepared by ultramicrotoming thin sections of about 70 nm thick with a diamond knife. These thin sections were then captured on carbon-coated copper grids for the observations.

2.3.7. BET surface area measurements

Adsorption and desorption isotherms for nitrogen were obtained at 77 K using a Micromeritics ASAP 2010 apparatus. The samples were out-gassed at 373 K and 0.1 Pa for 14 h before measurements. Specific surface area values were computed using the BET (Brunauer–Emmett–Teller) equation with relative pressures in the 0.05–0.20 range.

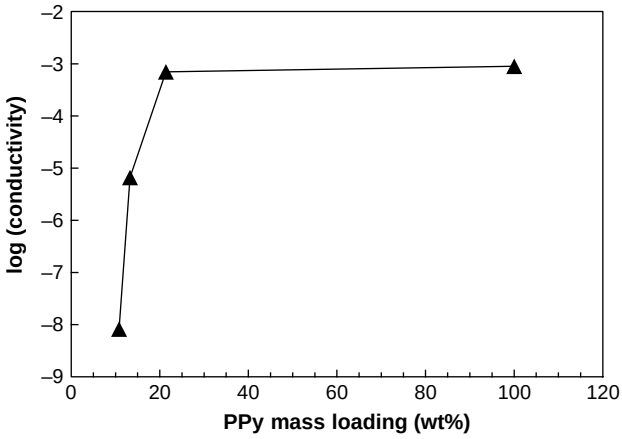

Fig. 1. Plot of the electrical conductivity (logarithmic values) of the MMT/PPy nanocomposites versus polypyrrole mass loading.

3. Results and discussion

3.1. Bulk chemical composition and conductivity

The initial pyrrole concentration was varied in order to obtain the PPy mass loadings 5, 10, 15 and 25 wt%. By determining the ratio of nitrogen weight percent in the MMT/PPy nanocomposites relative to that of the polypyrrole powder (15.9%), the real loadings of polypyrrole were found to be 2.8, 10.8, 13.3 and 21.4 wt%, respectively. Hereafter, the nanocomposites are abbreviated by MMT/PPy-*x*%, where *x* stands for the real PPy mass loading. The MMT/PPy nanocomposites are dark grey and eventually deep black coloured at high loadings (13.3 and 21.4%). The gradual incorporation of polypyrrole is reflected in the electrical conductivity measurements of the nanocomposite compressed pellets as shown in Fig. 1. The electrical conductivity sharply increases with polypyrrole loading until it reaches a plateau value matching that of bulk powder polypyrrole. In the case of MMT/PPy-2.8%, the conductivity was below the detection limit of the apparatus.

3.2. Morphology

SEM micrographs (Fig. 2) show that MMT has flaky particles arranged into the form of spheres with diameters up to 15 μm (Fig. 2a). At high maginification, PPy exhibits submicrometer-sized, bright globular particles (Fig. 2(b)). The morphology of the MMT/PPy-13.3% nanocomposite (Fig. 2(c)) differs slightly from that of the untreated clay (Fig. 2(a)) because the particles undergo some rearrangement of the original MMT flakes. Moreover, the surface exhibits some bright inclusions that could be assigned to polypyrrole as judged from Fig. 2(b). Indeed, it was shown elsewhere [22] that in the case of polypyrrole–polyurethane composites, the brighter the surface, the more conductive was the composite.

Contrary to what we have recently observed with PVC [34] or SiC [35] powder particle substrates, polypyrrole does not forms continuous coatings made of the individual spheres

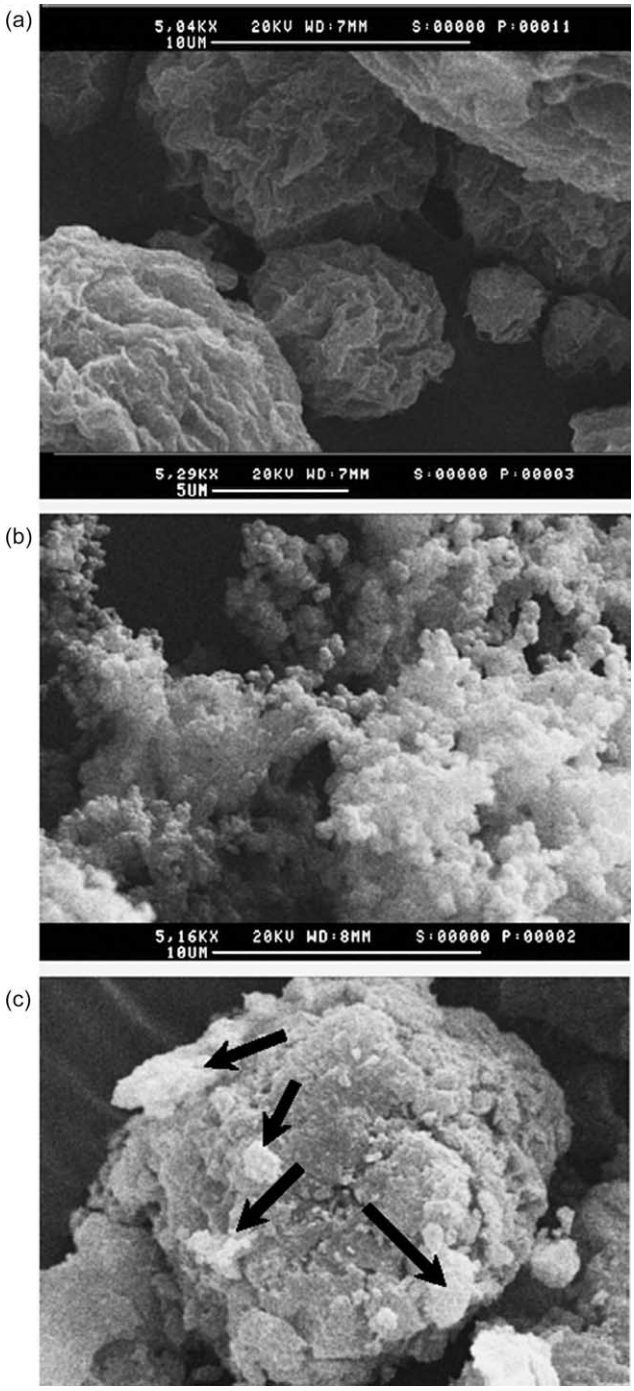

Fig. 2. SEM micrographs (magnification×5000) of (a) MMT, (b) PPy, and (c) MMT/PPy-13.3%.

shown in Fig. 2(b), but rather very thin layers topped with some patches (indicated by arrows in Fig. 2(c)).

3.3. Surface chemical composition

Fig. 3 shows the XPS survey scans of MMT/PPy-10.8% and the control MMT and PPy samples. The MMT/PPy-10.8% survey scan (Fig. 3(b)) is dominated by the main MMT features O1s (531 eV), Si2p (103 eV) and Al2p (74 eV), a qualitative indication that the nanocomposite surface is MMT-rich, and this actually holds for all MMT/PPy materials. This is similar to the cases of the microporous silica–PPy colloidal nanoparticles [36] and silica gel–polypyrrole composites [37], two types of materials which have silica-rich surfaces.

The apparent surface composition in atomic percent is reported in Table 1. The contributions of the major elements characteristic of polypyrrole, i.e. C and N, increase with polypyrrole loading, and simultaneously those of Si, Al and O (the major ones from the clay) decrease. Polypyrrole is thus gradually loaded at the surface of the nanocomposites as the initial pyrrole concentration increased. This is in line with the substantial increase in conductivity of the nanocomposites with PPy mass loading on the one hand, and the observation by SEM of the inclusions at the surface of MMT/PPy and which were assigned to PPy, on the other hand. However, the surface N/Si ratios 0.04, 0.05, 0.06 and 0.11 determined for polypyrrole mass loadings of 2.8, 10.8, 13.3 and 21.4%, respectively, are lower than those determined for the bulk of the nanocomposites by elemental analysis (with the exception of MMT/PPy-2.8%), i.e. 0.03, 0.12, 0.16 and 0.28, respectively. Therefore, polypyrrole is essentially confined in the interlamellar space of the clay particles.

It is worth to note that bulk powder polypyrrole is free from potassium whilst the nanocomposites have a substantial amount of this cation. The XPS detection of potassium in the nanocomposites highlights a cation-exchange phenomenon that involves Na^+ from the MMT substrate. Indeed, the wide scan in Fig. 3(b) (MMT/PPy-10.8%) indicates that the Na1s and NaKLL peaks are strongly attenuated compared to Si2p. To illustrate this ion-exchange, the surface (Na + K)/(Si + Al + Mg) atomic ratio was determined for untreated MMT and MMT/PPy specimens (Fig. 4). The ratio is invariably lower than that determined for the untreated MMT. This suggests a partial cation-exchange of Na^+ by K^+. Taking into account a contribution of 25–33% of positively charged nitrogen atoms in polypyrrole [33], still the (Na + K + N^+)/(Si + Al + Mg) atomic ratio is lower than that of MMT. It follows that the positively charged PPy backbone is also involved in the cation-exchange process, and that it 'sticks' to the host mineral material via electrostatic interactions. This has been discussed elsewhere for clay nanocomposites with conventional cationic polymers (e.g. polymer of β-dimethyl-aminoethylmethacrylate hydroacetate) [38], and conducting polyaniline [19] and polythiophene [21].

3.4. TEM measurements on the nanocomposites

Transmission electron microscopy (TEM) was used in order to confirm the polypyrrole intercalation on the basis of the assessment of the clay interlamellar spacing [11]. Fig. 5 shows that MMT has several sheets that can coil up at the edges (Fig. 5(a)). The preparation of the TEM samples by ultramicrotom permits to cut the clays perpendicularly to the sheet surfaces and, therefore, image the stacked layers. In the case of MMT/PPy-10.8%, Fig. 5(b) shows that the interlamellar spacing, 13.7 nm, is significantly higher compared to that of the untreated MMT (1.25 nm, see Fig. 5(a)). However, the intercalation of polypyrrole is not

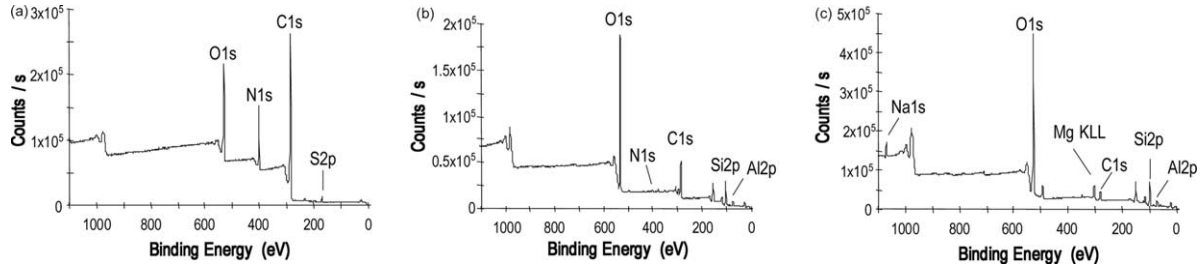

Fig. 3. XPS survey spectra of PPy (a), MMT/PPy-10.8% (b), MMT (c).

Table 1
Apparent surface chemical composition of the MMT/PPy nanocomposites and the reference materials MMT and PPy

Materials	C	N	O	Al	Si	Na	Fe	Ca	Mg	S	K
MMT	6.5	–	55.8	7.49	23.0	4.26	0.53	0.04	2.21	–	–
MMT/PPy-2.8%	9.6	0.95	54.8	8.35	22.8	0.33	0.50	0.0	1.47	0.08	1.10
MMT/PPy-10.8%	11.1	1.11	54.2	6.10	22.0	0.39	0.35	0.09	1.10	1.08	2.40
MMT/PPy-13.3%	11.5	1.30	53.7	6.13	21.7	0.27	0.37	0.11	1.04	1.31	2.57
MMT/PPy-21.4%	13.8	2.35	52.6	6.51	21.5	0.08	0.32	0.06	1.36	0.47	1.00
PPy	71.6	12.6	14.6	–	–	–	–	–	–	1.26	–

systematically homogeneous as some stacked sheets remain unmodified with practically the same spacing (1.25 nm) as in MMT, while others are filled with the polymer and have a spacing in the 1.58–18.96 nm range (Fig. 5(c)).

3.5. Surface energy and specific surface area

γ_S^d, the dispersive contribution to the surface energy was determined for the nanocomposites and the reference MMT and pure PPy using the well known method of Dorris and Gray [39]. γ_S^d values can be deduced from the ΔG_a, the free energy of adsorption of molecular probes, or more simply from the $RT\ln(V_N)$ values, where R is the gas constant, T the column temperature and V_N, the net retention volume of the molecular probes.

Fig. 6 depicts plots of $RT\ln(V_N)$ values versus the number of carbon atoms in the *n*-alkanes for PPy, MMT, and MMT/PPy-21.4%. The plots generate excellent linear correlations the slope of which equal to $\Delta G_a^{CH_2}$, i.e. the free energy of adsorption per CH_2 increment in the *n*-alkane series.

γ_s^d values were determined by IGC for the MMT/PPy nanocomposites, and the untreated host MMT at 150 and 180 °C (Table 2), a range of temperature used for the preparation of filled polyethylene and polypropylene composites prepared by melt mixing or by extrusion [6,40]. For untreated MMT, the γ_s^d value of 114 mJ/m^2 is slightly lower than the value of 155 mJ/m^2 obtained by Bandosz et al. for a Na-montmorillonite at 150 °C [41], however, after a thorough 15 h activation at 200 °C. It follows that the increase of the surface energy of MMT with temperature denotes most

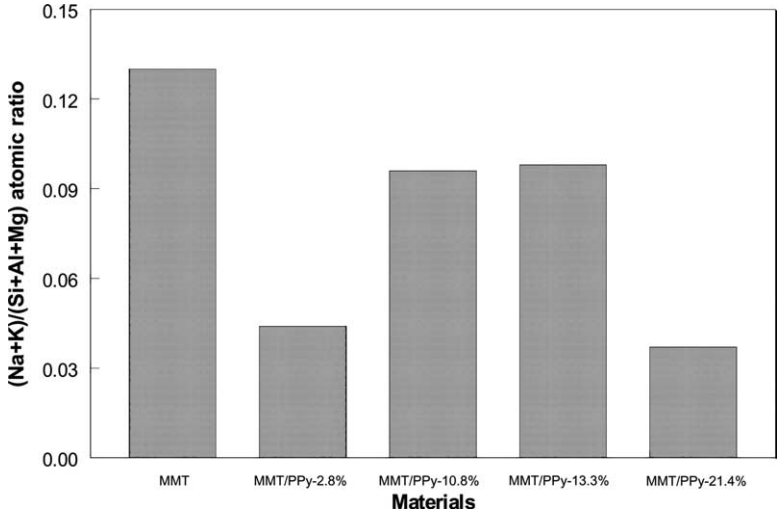

Fig. 4. (Na + K)/(Si + Al + Mg) atomic ratio determined by XPS for MMT and MMT/PPy nanocomposites.

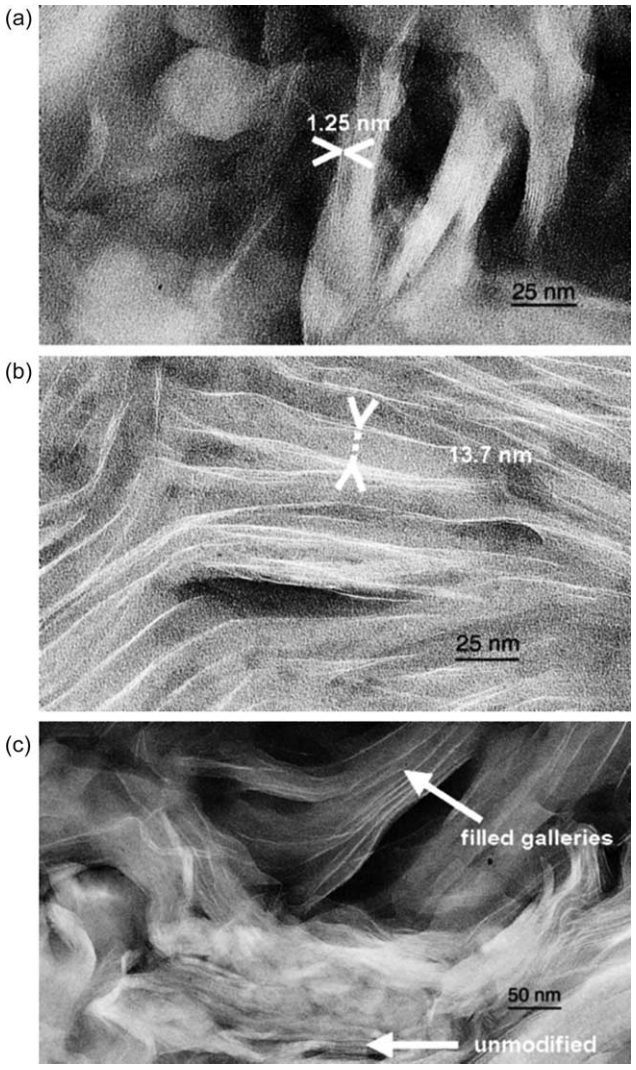

Fig. 5. Transmission electron micrographs of (a) MMT, (b) MMT/PPy-10.8%, and (c) MMT/PPy-10.8% showing unmodified and galleries filled by polypyrrole.

probably an activation of the clay surface. This has also been reported for illites and kaolinites [42], and sepiolite [43].

As far as the nanocomposites are concerned, PPy was expected to minimize the surface energy of MMT as in the case

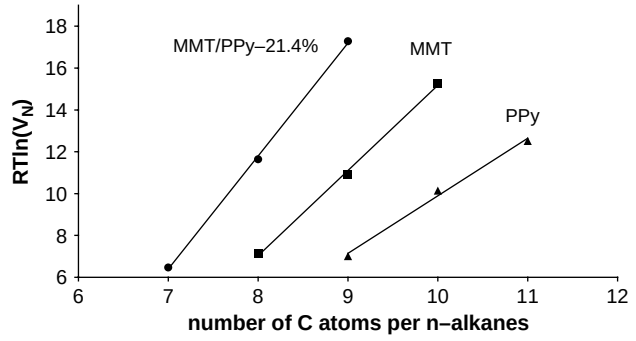

Fig. 6. Plots of $RT\ln(V_N)$ values vs. the number of carbon atoms in the *n*-alkane series injected in columns packed with PPy (at 80 °C), MMT and MMT/PPy-21.4% at 150 °C.

Table 2
γ_S^d values determined by IGC for MMT, PPy and MMT/PPy nanocomposites

Materials	γ_S^d(mJ/m^2)	
	150 °C	180 °C
MMT/PPy-2.8%	166	114
MMT/PPy-10.8%	159	142
MMT/PPy-13.3%	148	126
MMT/PPy-21.4%	199	180
MMT	114	134
PPy	45.1[a]	

[a] Determined at 80 °C. Attempts to determine retention times of probes injected in PPy-packed columns at 150 or 180 °C were actually unsuccessful due to the very fast elution at high temperature.

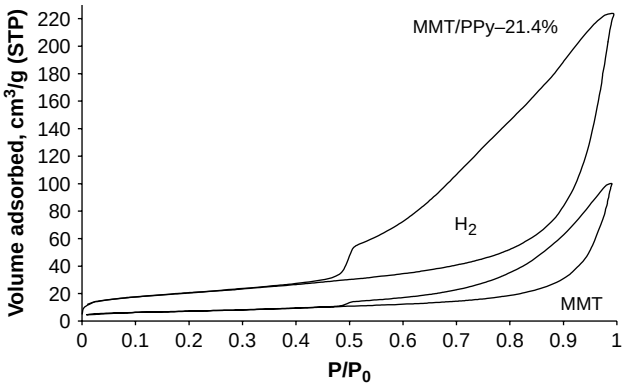

Fig. 7. Nitrogen isotherms obtained at 77 K for the montmorillonite reference material MMT and for MMT/PPy-21.4%.

Table 3
Specific surface areas (A_s) and C_{BET} values obtained for the pure MMT and the MMT/PPy nanocomposites

Materials	A_s (m^2/g)	C_{BET}
MMT	25.3±0.1	280
MMT/PPy-2.8%	32.8±0.1	179
MMT/PPy-10.8%	22.9±0.1	109
MMT/PPy-13.3%	20.3±0.1	102
MMT/PPy-21.4%	73.3±0.1	127

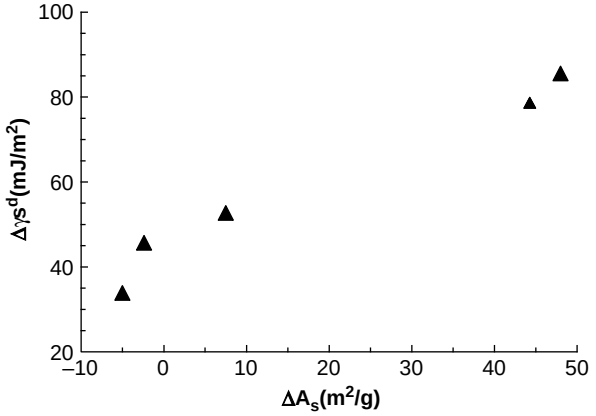

Fig. 8. Plot of $\Delta\gamma_s^d$ (at 150 °C) versus ΔA_s for the MMT/PPy nanocomposites.

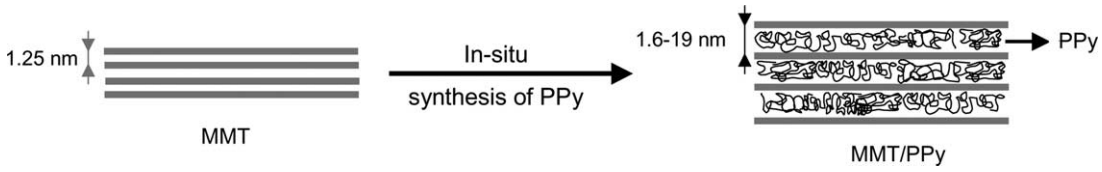

Fig. 9. Schematic representation of polypyrrole intercalation in the MMT galleries.

of MMT–polystyrene sulfonate [41]. However, the MMT γ_s^d value is rather increased after intercalation of PPy. Therefore, IGC provides important information on the structural changes of the host MMT. As in the case of the microporous silica/PPy nanocomposites [32], the MMT/PPy materials have a much higher surface energy than their components taken separately. It is possible that this is driven by the insertion phenomena experienced by linear alkanes when probing microporous or lamellar materials [44]. In addition, the increase in the surface energy for a given material may parallel changes in the specific surface area [24].

In the context of this work, the specific surface areas were determined from the nitrogen adsorption isotherms and application of the classical Brauner–Emmet–Teller (BET) equation to the adsorption data. The isotherms obtained for the pure MMT and the MMT/PPy-21.4% are presented in Fig. 7. Interestingly, the hysteresis observed for the nanocomposite is much more pronounced than that obtained in the case of MMT, thus reflecting a massive adsorption of nitrogen. These isotherms cannot be considered as of the type IV (i.e. existence of mesopores) since no plateau can be reached at high relative pressure excluding the completion of mesopore filling. All materials under test are rather characterized by a type IIb isotherm (i.e. observed with platy particles) and exhibit a hysteresis loop of type H3 [45]. Note that this H3 loop is related to adsorbents containing slit-shaped pores or to aggregates of platy particles [46].

Table 3 reports the specific surface area (A_s) and the BET constants (C_{BET}) for MMT and MMT/PPy nanocomposites. One can see that there is a dramatic increase A_s for a high loading of PPy (e.g. 21.4 wt%). This is in line with a study of MMT–iron oxide nanocomposites [47]. However, the data in Table 3 show that there is no obvious correlation between polypyrrole loading and the A_s value. Nevertheless, one can tentatively relate the changes in the surface energy and surface area ($\Delta\gamma_s^d$ and ΔA_s, respectively) of MMT. These parameters are defined as:

$$\Delta\gamma_S^d = \gamma_S^d(\text{MMT/PPy}) - \gamma_S^d(\text{MMT})$$

and

$$\Delta A_s = A_s(\text{MMT/PPy}) - A_s(\text{MMT})$$

Fig. 8 displays a plot of $\Delta\gamma_s^d$ at 150 °C versus ΔA_s for the MMT/PPy nanocomposites. The results show that the increase in the surface energy correlates with the increase in the specific surface area as found elsewhere for example heat-treated silica materials [48].

Using the C_{BET} constants in Table 3, the net molar energy of adsorption ($E_1 - E_L$) can be calculated using:

$$C_{BET} \approx \exp\left(\frac{E_1 - E_L}{RT}\right)$$

where E_1 and E_L stand for the isosteric heat of adsorption and for the liquefaction energy, respectively. The incorporation of the polymer leads to a significant decrease of the C_{BET} parameter (Table 3), compared to MMT. Considering that a high value of the C_{BET} parameter is an indication of the presence of microporosity, it seems that the nanocomposites exhibit a less developed microporosity. This contrasts with the γ_s^d values which are higher for the nanocomposites compared to the pure MMT, expressing stronger interactions of the *n*-alcanes with the formers than with the latter.

It is possible that when PPy is intercalated in MMT, it modifies the interlayer structure in such a way that the filling is only partial (see for example Fig. 5(c)) so that new voids or tunnels are created in which *n*-alcane adsorption sites of higher energy are generated. Therefore, any *n*-alkane that probes these accessible sites remains strongly retained inside the nanocomposite, hence the increase in the relative retention times and the subsequent increase in γ_s^d. In the same time, the intercalation of PPy leads to a partial blocking of the micropores, hence the decrease in C_{BET} for high polypyrrole loading.

On the basis of the results and discussion above, Fig. 9 schematically illustrates the intercalation of polypyrrole in the galleries of the host MMT.

4. Conclusion

Montmorillonite/polypyrrole nanocomposites with polypyrrole mass loadings ranging from 2.8 to 21.4 wt% were prepared and characterized in terms of microscopic morphology, surface chemical composition, surface energy and specific surface area. XPS showed that cation exchange phenomena occurred during the in situ synthesis of polypyrrole involving potassium from the oxidizing agent ($K_2S_2O_8$) of pyrrole and also the PPy positively charged backbone. In addition, the surfaces of the nanocomposites are montmorillonite-rich due to the intercalation of polypyrrole in the MMT galleries. This intercalation resulted in a significant increase of the clay interlamellar spacing that was directly observed by means of TEM. The intercalated PPy imparts to the host MMT a high dispersive contribution to the surface energy and a high specific surface area, therefore, emphasizing significant changes in the structure and adsorption properties of the mineral material.

Acknowledgements

The authors would like to thank the CNRS and the Slovak Academy of Science for financial support through the bilateral

French-Slovak cooperation (project number 14429), the Science and Technology Assistance Agency APVT 51-01852, Slovakia, and the SESAME 2000 scheme (Conseil Régional d'Ile-de-France). Mrs M.-J. Vaulay is acknowledged for her assistance with SEM studies.

References

[1] Aldissi M, editor. Intrinsically conducting polymers: an emerging technology. Dordrecht: Kluwer; 1993.
[2] Nalwa HS, editor. Handbook of organic conducting molecules and polymers, vol. 2. Chichester: Wiley; 1997.
[3] Skotheim TA, Elsenbaumer RL, Reynolds JR, editors. Handbook of conducting polymers. 2nd ed.. New York: Marcel Dekker; 1998.
[4] Rodriguez J, Grande H, Otero TF. Handbook of organic conducting molecules and polymers, vol. 2. Chichester: Wiley; 1997 p. 415–68.
[5] Armes SP. Handbook of conducting polymers. 2nd ed. New York: Marcel Dekker; 1998 p. 423–5 [Chapter 17].
[6] Omastova M, Pionteck J, Kosina S. In: Hotta S, editor. Electronic and optical properties of conjugated molecular systems in condensed phases. Kerala, India: Research Signpost; p. 153–86.
[7] Hasegawa N, Okamoto H, Kawasumi M, Kato M, Tsukigase A, Usuki A. Macromol Mater Eng 2000;180–181:76.
[8] Alexandre M, Dubois P. Mater Sci Eng 2000;28:1.
[9] Garcia-Lopez D, Picazo O, Merino JC, Pastor JM. Eur Polym J 2003;39:945.
[10] Sinha Ray S, Biswas M. Mater Res Bull 1999;34:1187.
[11] Hong SH, Kim BH, Joo J, Kim JW, Choi HJ. Curr Appl Phys 2001;1:447.
[12] Omastová M, Mravčáková M, Pionteck J, Chodák I. Proc Nanocompos 2003 [San Francisco, CA, USA].
[13] Oriakhi ChO, Lerner MM. Mater Res Bull 1995;30:723.
[14] Yeh JM, Chin ChP, Chang S. J Appl Polym Sci 2003;88:3264.
[15] Park DP, Sung JH, Lim ST, Choi HJ. J Mater Sci Lett 2003;22:1299.
[16] Kim JW, Liu F, Choi HJ, Hong SH, Joo J. Polymer 2003;44:289.
[17] Sinha Ray S, Okamoto M. Prog Polym Sci 2003;28:1539.
[18] Letaïef S, Aranda P, Ruiz-Hitzky E. Appl Clay Sci 2005;28:183.
[19] do Nascimento GM, Constantino VRL, Landers R, Temperini MLA. Macromolecules 2004;37:9373.
[20] Lee D, Char K, Lee SW, Park YW. J Mater Chem 2003;13:2942.
[21] Ballav N, Biswas M. Synth Met 2004;142:309.
[22] Ruckenstein E, Chen JH. Polymer 1993;32:1230.
[23] Omastovtá M, Pionteck J, Kosina S. Eur Polym J 1996;32:681.
[24] Ansari DM, Price GJ. Polymer 2004;45:3663.
[25] Mamunya Y. Macromol Symp 2001;170:257.
[26] Belgacem MN, Gandini A. In: Pefferkorn E, editor. Interfacial phenomena in chromatography (surfactant science series), vol. 80. New York: Marcel Dekker; 1999. p. 41–124.
[27] Chehimi MM, Azioune A, Cabet-Deliry E. In: Mittal KL, Pizzi A, editors. Handbook of adhesive technology. New York: Marcel Dekker Inc.; 2003. p. 95–144 [Chapter 5].
[28] Chehimi MM, Abel M-L, Perruchot C, Delamar M, Lascelles SF, Armes SP. Synth Met 1999;104:51.
[29] Chehimi MM, Abel M-L, Sahraoui Z. J Adhes Sci Technol 1996;10:287.
[30] Abel M-L, Chehimi MM, Fricker F, Delamar M, Brown AM, Watts JF. J Chromatogr 2002;A969:273.
[31] Ben Slimane A, Boukerma K, Chabut M, Chehimi MM. Colloids Surf A 2004;240:45.
[32] Perruchot C, Chehimi MM, Delamar M, Lascelles SF, Armes SP. J Colloid Interface Sci 1997;193:190.
[33] Kang ET, Neoh KG, Tan KL. Adv Polym Sci 1993;106:135.
[34] Ben Slimane A, Chehimi MM, Vaulay M-J. Colloid Polym Sci 2004;282:314.
[35] Omastová M, Boukerma K, Chehimi MM, Trchová M. Mater Res Bull 2005;40:749.
[36] Azioune A, Ben Slimane A, Ait Hamou L, Pleuvy A, Chehimi MM, Perruchot C, et al. Langmuir 2004;20:3350.
[37] Perruchot C, Chehimi MM, Delamar M, Fievet F. Surf Interface Anal 1998;26:689.
[38] Theng BKG, editor. Formation and properties of clay–polymer complexes. Developments in soil science, vol. 9. Amsterdam: Elsevier; 1979 [Chapter 5].
[39] Dorris GM, Gray DG. J Colloid Interface Sci 1980;77:353.
[40] Karger-Kocsis J, editor. Polypropylene an A–Z reference. Dordrecht: Kluwer Academic Publishers; 1998.
[41] Bandosz TJ, Putyera K, Jagiełło J, Schwarz JA. Microporous Mater 1993;1:73.
[42] Saada A, Papirer E, Balard H, Siffert B. J Colloid Interface Sci 1995;175:212.
[43] Morales E, Dabrio MV, Herrero CR, Acosta JL. Chromatographia 1991;31:357.
[44] Papirer E, Balard H. In: Pefferkorn E, editor. Interfacial phenomena in chromatography (surfactant science series), vol. 80. New York: Marcel Dekker; 1999. p. 145–71.
[45] Rouquerol F, Rouquerol J, Sing K. Adsorption by powders and porous solids. London: Academic Press; 1997 p. 364.
[46] Rouquerol F, Rouquerol J, Sing K. Adsorption by powders and porous solids. London: Academic Press; 1997 p. 205.
[47] Oliveira LCA, Rios RVRA, Fabris JD, Sapag K, Garg VK, Lago RM. Appl Clay Sci 2003;22:169.
[48] Linger G, Vidal A, Balard H, Papirer E. J Colloid Interface Sci 1989;133:200.